http://dx.doi.org/10.21577/0103-5053.20190020

J. Braz. Chem. Soc., Vol. 30, No. 6, 1252-1265, 2019
Printed in Brazil - ©2019 Sociedade Brasileira de Química

Article

Reduction of Aqueous Ag^+ Steered by Electrochemical Plasma: Connecting the Bulk pH Variation with the Reaction Pathways for Hydrated Electrons

Ingrid A. Gonçalves,[a] Jairo Barauna,[a] Fernando J. Cunha-Filho,[b] Osvaldo Chiavone-Filho,[b] Jussier O. Vitoriano,[a,c] Clodomiro Alves Júnior[a,c] and Andressa Mota-Lima[*,b,d]

[a]*Laboratório de Plasma Aplicado a Agricultura, Saúde e Meio Ambiente, Universidade Federal Rural do Semiárido, 59625-900 Mossoró-RN, Brazil*

[b]*Departamento de Engenharia Química, Universidade Federal do Rio Grande do Norte, Av. Sen. Salgado Filho, 3000, 59078-970 Natal-RN, Brazil*

[c]*Departamento de Engenharia Mecânica, Universidade Federal do Rio Grande do Norte, Av. Sen. Salgado Filho, 3000, 59078-970 Natal-RN, Brazil*

[d]*Programa de Pós-Doutorado em Engenharia Química, Escola Politécnica da Universidade de São Paulo, Rua do Largo, 250, 05508-080 São Paulo-SP, Brazil*

Reduction of silver cations followed by nanoparticle (Ag-NPs) synthesis is a model process to understand the reduction mechanism induced by a discharge over an aqueous surface, termed electrochemical plasma. This work aims at studying the silver reduction reaction steered by electrochemical plasma in the presence of other chemically active plasma-related interfaces, namely the plasma-gas and the liquid-gas interfaces. As no other plasma-induced species are able to reduce silver cations, the reduction of silver cations is employed as strategy to selectively detect the presence of hydrated electrons (e_h^-). The results demonstrate that the global rise of pH (increase in the content of OH^-), observed for discharge in the helium gas phase, occurs in connection with the silver reduction, which is interpreted as a vivid experimental evidence of the second-order recombination reaction of the e_h^- ($2e_{aq}^- + 2H_2O \rightarrow H_2 + 2OH^-$). On the other hand, the global decrease of pH (increase in the content of H^+) observed for discharge in mixed oxygen and nitrogen gas phase, is an event primarily driven by the Birkeland-Eyde process, and it is concomitant but spatially distinct from the electron injection. The acidification interferes in the NP formation, as NPs promptly dissolve in presence of HNO_3. Only in complete suppression of the acidification, an experimental evidence of the reaction pathways for hydrated electron could be captured: e_h^- is competitively consumed through a scavenger-like reaction (reduction of silver cations in this work) and through the second-order recombination reactions of the e_h^-. The kinetic model proposed in this work further corroborates this interpretation.

Keywords: Ag NPs synthesis, electrochemical plasma, hydrated electrons, glow discharge, DBD, jet plasma

Introduction

The capability of atmospheric-pressure plasma to promote electrons and ions in the gas leads to a net flow of charges through the plasma-liquid interface (PLI), driving electrochemical reactions in the liquid phase.[1-4] The promotion of electrochemical reaction on the liquid phase has launched new routes of plasma-based synthesis, which includes, among few examples, the synthesis of nanosized noble metals[5-17] and oxides[18-22] plus the synthesis of liquid fuels via CO_2 reduction.[23] However, the underlying mechanism of plasma-induced synthesis is poorly understood and, from an electrochemical perspective, it involves the clarification of two fundamental aspects: (*i*) the nature of the charge carrier and its mechanism of transfer through the PLI; and (*ii*) the reducing mechanism in the liquid phase. In this Introduction section, the literature is surveyed to tentatively shed light into these two fundamental points. Furthermore, we survey the most relevant chemical interactions promoted by the other

*e-mail: mota@usp.br

chemically active interfaces related to the PLI, namely the plasma/gas and gas/liquid interfaces.

Charge transfer through PLI is experimentally investigated by measuring the current through any point on the external circuit with respect to the plasma; in this regard, literature has insipient electrical data describing the charge transfer for the PLI. In reference to the nature of the charge carrier through the PLI, either electrons or mass-containing charge carriers demonstrate to effectively cross the PLI. To date, electron uptake by the liquid phase has been observed mainly for negative plasma (cathodic plasma)[1,24] and more rarely for positive plasma (anodic plasma),[25] while uptake of aqueous cations by the plasma phase has been observed solely for anodic plasma.[26] Thus, Bruggeman *et al.*[27] thoroughly evaluated the plasma species crossing the PLI; in the meantime Chen *et al.*[28] provided a survey on the polarity effect on the processes at PLI, discussing the effects of accelerated electrons and ions toward the liquid. A second aspect to tackle the understanding about the charge transfer involves the experimental access to faradaic current *versus* potential (j_F *vs.* U) curves. In this context, Hickling and Ingram[29] along with Sengupta *et al.*[30,31] observed that conventional water electrolysis obeys the Faraday law once the interfacial potential remains below the breakdown potential. So far, a comprehensive review of the main characteristics of j_F *vs.* U curves for contact (inside liquid) and contactless (over liquid) glow discharge is provided by Akolkar and Sankaran.[32]

The reducing reaction of a metallic cation, followed by its accretion and nanoparticle synthesis has been employed as a model process for studying the mechanism of reduction induced by plasma. Currently, two reducing agents have been extensively considered for reducing gold cations: hydrated electrons (e_h^-, electrons solvated by water molecules) and hydrogen peroxide (H_2O_2). They are synthesized via independent routes: synthesis of H_2O_2 depends on an initial step based on a plasma neutral reaction,[33-35] whereas the free electrons in the plasma are directly accelerated toward the liquid surface, injecting e_h^- in the liquid phase. The e_h^- are short-lived species that readily reacts via second-order recombination reaction.[36] By contrast, H_2O_2 is long-lived specie selectively produced by anodic polarity in an electrochemical plasma.[34] An attempt to estimate the major reducing species in liquid phase would be drawn by analyzing their yields of production. However, yield of e_h^- in the electrochemical plasma remains lacking. With respect to the yields for plasma-generated H_2O_2, Locke and Shih[35] concluded that all discharge sources (radio-frequency (RF), pulsed, alternating current (AC) or direct current (DC)) and configurations (contact or contactless plasma) exhibit yields in the range of 4×10^{-2} to 80 g kWh^{-1}. Last but not least, the nature of the metallic cations must be considered when sorting candidates for the list of reducing agent. Hydrogen peroxide does not reduce silver cations in water because silver peroxides are formed. On the other hand, gold cations are reduced either by hydrogen peroxide or by hydrated electrons. In this scenario, the usage of silver cations is employed as a strategy to the selective detection of hydrated electrons.

Within the span of discharge, three phases co-exist: the plasma, gas and liquid phases. The boundaries between these three phases define conceptually three interfaces: (*i*) the plasma-gas interface, labeled as the "plasma edge"; (*ii*) the gas-liquid interface that is rich in species carried by the plasma effluent; and (*iii*) the PLI. Several other processes, beyond electro-reduction in the liquid region underneath the PLI, develop on the other plasma-related interfaces. For example, the plasma edge is a reactive interface when in the presence of relative proportions between N_2:O_2 that according to Schmidt-Bleker *et al.*[37] produces long-living species. Presumably, the species detected by Schmidt-Bleker *et al.*[37] could lead to the acidification of the bulk liquid as it had been reported for either cathodic[38] or anodic[39] plasma polarities. If so, the gas/liquid interface participates actively on the physical-chemical changes of the liquid phase. Further example is related to the peroxide synthesis in plasma phase whose liquid absorption substantially increases if the gas/liquid area enlarges by means of using water droplets (aerosol inside plasma).[35] Several other short-lived species ($OH^•$ radical, $H^•$ radical and superoxide) were detected in liquid phase by Gorbanev *et al.*[40] that used a torch-like to demonstrate the liquid uptake of the plasma-synthesized species via interaction of the plasma effluents with the liquid surface. A second and less-mentioned macroscopic phenomenon related to the gas-liquid interface is the charge transport induced by an electric field throughout the gas phase. Bednar *et al.*[41] demonstrated that the current of plasma-induced-charged species in the gas phase are sensitive to the applied electric field.

Regarding the plasma-liquid interface, two macroscopic changes in the liquid phase have been reported some time after discharge: electro-reduction reactions and H_2O_2 synthesis. Several reduction-like reactions have been reported majorly for cathodic plasma: CO_2 reduction,[23] hydrogen evolution reaction,[41,42] ferricyanide reduction[2] and metallic cation reduction.[3] The reduction capability of the anodic plasma was confirmed by a single work, employing the reduction of monochloroacetic acid.[25] The presence of H_2O_2 has also been detected[31,33,34,43] and demonstrated to be exclusively synthesized by anodic plasma. Glasstone and Hickling[33] suggested that H_2O_2 is produced by the action

of electrical discharge on water vapor. When in absence of water vapor, Liu *et al.*[34] proposed that water molecules in the plasma phase are the result of processes related to the anodic sheath over liquid (sputtering, electric field induction ion emission and evaporation), and for this reason, cathodic plasma polarization (for which the anodic sheath is not over liquid) tends to lack H_2O_2 production. Hitherto, the plasma polarity assumes a selective function towards the macroscopic effect on the plasma-liquid interface, i.e., cathodic plasma promotes the reduction reaction mediated by e^-_{aq}, and anodic plasma promotes H_2O_2 synthesis.

Among several atmospheric-plasma sources (transferred arcs, plasma torches, corona discharge and dielectric barrier discharges (DBD)), only a few have been used to modify the properties of a water surface.[32,44] In particular, the present work considers the impact of the atmosphere composition on the ability of two types of plasma sources to promote silver reduction in aqueous phase. The results aid to partially dissipate the fog covering the fundamental understanding on the plasma-induced reduction mechanism in liquid phase, i.e., in the presence of other chemically active plasma-related interfaces, namely the plasma-gas and the liquid-gas interfaces.

Experimental

Two different plasma sources were tested in this work to generate atmosphere plasmas over a liquid surface: glow discharge (GD) and dielectric barrier discharge with jet effect (DBD-Jet). These sources were combined with different gaseous composition as shown in Figure 1. The discharge is initiated at the tip electrode, given the concentrated electrical field on its surroundings, and propagates toward the flat surface of water which performs as counter electrode, dragging the charges that flows into the plasma/liquid interface. The discharge is known to be GD when a narrow wire is used as tip electrode. In this work, we used a stainless-steel tip (diameter of 0.01 m) located approximately 5 mm above the electrolyte, with a slightly static gas phase (15 sccm) filled either by air or helium, see Figures 1a and 1b. When a metallic ring grasping the outside walls of a hollow glassy tube (inner diameter of 1.3 mm) is used with inner flow of helium at 1000 sccm, the discharge is said to be jet dielectric barrier discharge (DBD-Jet); see sketch in Figure 1c. The discharges were labeled as cathodic plasma as the tinny tip electrode was connected to the negative terminals of the high voltage power supply. Table 1 summarizes the three experimental system used in this work, emphasizing details about different fluid-dynamics.

A homemade pulsed high voltage embeds a power supply into an integrated electrical circuit whose function is to create a pulse of high voltage. A typical pulse is shown in Figure 2 for a cathodic polarization. For this particular recorded pulse, the peak-to-peak potential is 7.6 kV and frequency is 588 Hz. These values poorly describe the temporal evolution of the pulsed potential. Ideally, full temporal evolution of potential would have to be recorded, but we were unable to accomplish given the limited data acquisition of our oscilloscope. Instead, several snapshots of the oscilloscope screen were analyzed to attemptedly build a mean average and mean variance for the peak-to-peak and frequency: 7.0 ± 2.5 kV and 550 ± 30 Hz, respectively. The uncertainty on these values is connected to the inherent dynamic evolution of the electrical variables (current and potential) for the equivalent circuit of the plasma.

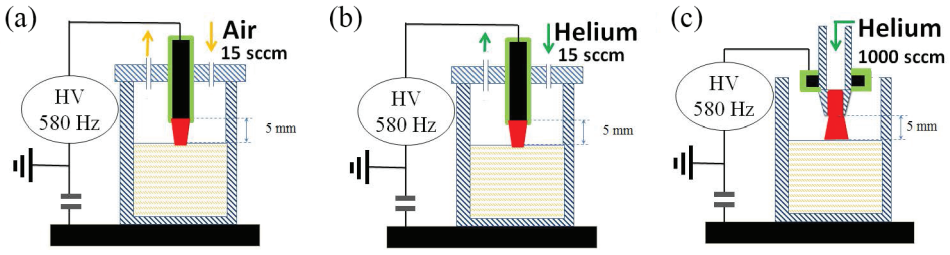

Figure 1. Experimental setups for generating plasma in the gas phase but over a liquid surface: (a) GD-air; (b) GD-He and (c) DBD-(He)Jet in air, using cathodic polarity (negatively biased). Black = metallic electrode; red = plasma; blue = silicate glass (dielectric material); green = polymer isolator.

Table 1. Plasma sources combined with different gas/plasma fluid-dynamics

Plasma source (label)	Composition at plasma edge[a]	Effluent flux / sccm	Effluent phase
Glow discharge (GD-air)	air/air	15	gas
Glow discharge (GD-He)	He/He	15	gas
Dielectric barrier discharge with jet effect (DBD-(He)Jet)	air/He	1000	plasma

[a]Plasma edge is the interface gas/plasma.

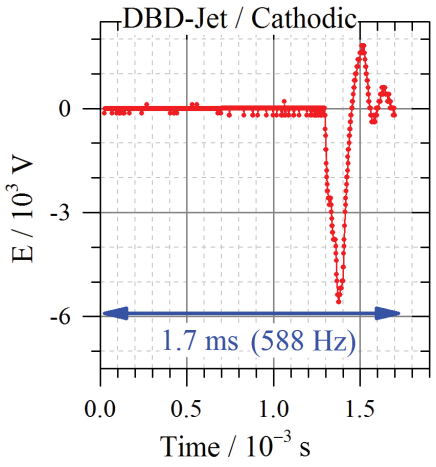

Figure 2. Time evolution of the electrical potential applied between the two electrodes for a single pulse in a DBD-Jet using cathodic polarization.

The electrolyte was prepared with bi-distilled water, 2 mM of silver nitrate ($AgNO_3$, Sigma-Aldrich) and 1% m/m trisodium citrate ($Na_3C_6H_5O_7$, Proquimicos). All experiments used 4.2 mL of electrolyte. The values of pH (Oakton PC450 meter and an SJ pH/ATC probe) were measured before and after treatment. To measure the pH, the entire electrolyte volume was used by simply immersing the pH electrode after treatment. Each measurement was repeated three to four times. The visualization of the nanoparticle was carried out with a high resolution transmission electronic microscopy (TEM, Tecnai G2 F20-FEG). The sample preparation includes the deposition of a polymeric film over the finer mesh TEM grids in a first step, and the deposition of the nanoparticles upon the polymeric film in a second step. The first and second steps include the drip of a polymeric solution and an ultrasound-treated Ag nanoparticle (Ag-NP) suspension, respectively; each step is followed by a drying period in a closed chamber at room temperature.

Scilab,[45] which is a free and open-source software, was used to implement the numerical methods to solve the set of differential equations, that describes the mechanism of reaction for the hydrated electrons. The computational experiments were carried out on a five-core machine with 64-bits architecture running Windows operating system. Fourth order Runge-Kutta method were selected as the interactive method, and the code were solved for different initial conditions.

Results and Discussion

NP synthesis in presence of air or helium in the plasma edge

Figure 3 shows the pH and UV-Vis absorbance spectra for $AgNO_3$ solutions measured simultaneously for three different plasma sources, using cathodic polarization within 15 min. As a general observation for air-containing plasma edge, either DBD-Jet or GD plasmas promote solution acidification (see Figures 3b and 3f). However, solely DBD-Jet effectively synthesizes NPs (see Figures 3a and 3e).

Synthesis of Ag-NPs with DBD-Jet is followed by slight acidification of the bulk electrolyte (Figure 3f), as the pH vary from 6.7 to 6.5 within 15 min of the DBD-Jet plasma treatment. Initially, the silver cation solution is translucent; during plasma treatment, it acquires a yellow color, reflecting the surface plasmon band (SPB)[46] that is characteristic of colloidal nanoparticle silver. In Figure 3e, a plasmon band at approximately 420 nm appears within the initial 5 min and grows in intensity within 15 min, indicating a progressive temporal increase of the NP concentration. Similar results have already been found in the literature considering spherical nanoparticles.[3,47-50] As the intensity relates to NP concentration, the larger absorbance intensity indicates that NPs are continuously nucleated, even at the later minutes. Finally, Figure 4 shows images of NPs formed after DBD-Jet treatment in an air-containing atmosphere, confirming Ag-NP synthesis.

Contrariwise, after treatment with air-GD, the absent NP formation, due to the conservation of the electrolyte translucence, confirms with UV-Vis data that exhibit negligible increase of the plasmon band at 420 nm, see Figure 3a. For comparison, the same Figure 3a also displays UV-Vis absorbance for an aqueous solution of pure $AgNO_3$ in addition to mixture solution of $AgNO_3$ plus citrate a day after its mixture. The synthesis of NP occurs for a solution without discharge treatment but in presence of citrate, because the citrate takes over the role of reducing agent. If the same electrolyte submits to GD-air during 15 min, a peak at 350 nm rises in addition to the plasmon peak at 420 nm. This new peak is interpreted as the plasmon band related to Ag-NPs with smaller diameter than Ag-NPs at 420 nm (the shoulder at 300 nm is attributed to the NO_3^- belonging to the initial solution). The observation of a shoulder at 350 nm in the UV-Vis absorption is relevant to this work as key evidence that the GD electrode reduces Ag^+ to Ag^0, although a minor net NP formation occurs. This result accompanies a very steep decrease of the solution pH from 6.7 to 4.0 within 15 min of air-GD treatment, see Figure 3b. This result clearly suggests that a faster acidification process inhibits the NP formation. It is well-known that nitric acid dissolves noble and non-noble metals, and its presence in liquid phase is attributed to the Birkeland-Eyde process (in the Birkeland original work)[51] that leads to nitrogen fixation as strong acid (nitric acid), resulting in the reduction of the

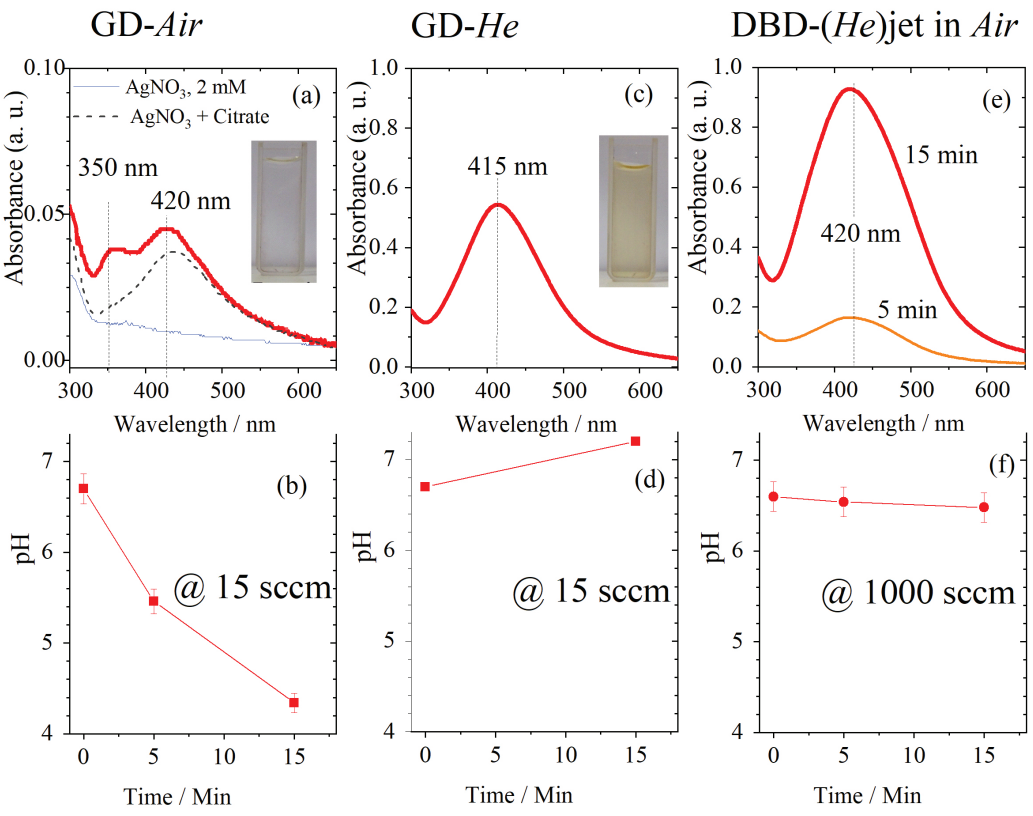

Figure 3. UV-Vis spectra (top row) and pH of the bulk electrolyte (bottom row) submitted to glow discharge (a-b) in the air or (c-d) in the helium, and DBD-Jet plasma (e-f) employing 1000 sccm of helium jet-flow. 4.2 mL volume of electrolyte and inserted images show the solution after treatment; for all the cases, the treatment lasted 15 min unless otherwise stated.

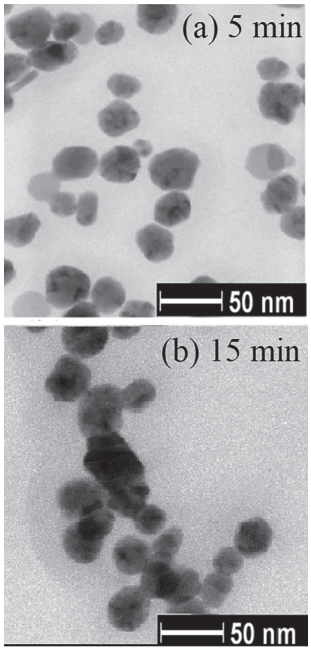

Figure 4. Bright field TEM images for NP synthesized with DBD-Jet plasma during (a) 5 and (b) 15 min under cathodic discharge.

pH. Making a parallel with metal reduction via a chemical route, a similar inhibition of formation of Ag-NPs is also reported in the presence of intentional addition of nitric acid[52] in the electrolyte before the synthesis. According to our interpretation, Ag^+ does is reduced when GD electrode is used, but Ag^0 accretes slowly due the presence of nitric acid in the aqueous media, which in turn results in an overall negligible nucleation rate.

To validate the hypothesis that acidification inhibits Ag-NP formation, GD was performed in a helium gas phase, i.e., in a complete absence of oxygen or nitrogen in the gas phase, thus completely suppressing the Birkeland-Eyde process. Using such experimental condition, NPs are formed, see Figure 3c; however, the bulk pH interestingly increases above 7, see Figure 3d. Notably, the rising pH is a relevant experimental piece because it indicates the presence of one product (OH^-) related to a parallel reaction with respect to the silver cation reduction (equation 1).

$$Ag^+ + e_h^- \xrightarrow{k1 = 3.7 \times 10^{10} M^{-1} s^{-1}} Ag^0 \quad (1)$$

The basification indicates the rise of OH^- content in the bulk liquid, which is interpreted in the context of recombination reaction between hydrated electrons (equation 2).[36]

$$2e_h^- + 2H_2O \xrightarrow{k2 = 5.5 \times 10^9 M^{-1} s^{-1}} H_2 + 2OH^- \quad (2)$$

The recombination reaction follows a poorly understood mechanism at atomistic level; it presumably proceeds via an activated complex generated by collision of two hydrated electrons, forming a singlet dielectron that readily reacts with the water molecules from the hydration sphere. The recombination reaction follows a second-order rate of reaction with respect to the concentration of hydrated electrons, implying that the rate of e_h^- consumption (or OH^- formation) is highly sensitive to the local concentration of hydrated electrons. The square dependence on the e_h^- concentration indicates that if an instantaneous concentration of the e_h^- is increased above the unit, the rate of second-order reactions (see equation 2) increases further than does a first order reaction (see equation 1).

The increased pH in conjunction with the NP synthesis, seen in Figures 3c and 3d, indicates that reaction on equation 2 had occurred concomitantly with the reaction on equation 1. Under the light of the findings of Gopalakrishnan *et al.*[24] and Rumbach *et al*.,[1] we propose that the increased pH is an important experimental evidence that electron had effectively being injected into the liquid phase during the discharge. Furthermore, the parallel effect of NP formation and OH^- production is interpreted in the context of the electrochemical concept of Faradaic efficiency. Despite having not measured the forced current flowing through the PLI, we argue that the net flow of electrons throughout the PLI (j_{PLI}) splits into two reaction channels, the flow of electrons related to the quantities of reduced silver cations (j_{NP}) plus produced OH^- (j_{OH}): $j_{PLI} = j_{NP} + j_{OH}$. This means that not all hydrated electrons react with the silver cation, resulting in a Faradaic selectivity for the cation reduction reaction below 100%, which is substantially consistent with the decreased Faradaic selectivity observed by Ghosh *et al.,*[55] which similarly used small silver cations concentrations. At this point of the analysis, we suspect that a rapid acidification rate not only inhibits the NP formation, but also hides the experimental perception about reaction 2, since all the locally-formed underneath-PLI OH^- is neutralized by the risen H^+ content.

To convince ourselves effectively, we tested a second strategy to further validate the hypothesis that the acidification inhibits Ag-NP formation. We tested the same apparatus used in Figures 3a and 3b, but departing from an electrolyte enriched with sodium hydroxide. If the initial electrolyte was basic instead of almost neutral, all embedded nitric acid would suffer a net neutralization reaction resulting in a nitrate salt instead of simply being dissolved as aqueous nitric acid. In fact, our experiment with intentionally-alkaline initial electrolyte acquired yellow color within 15 min under GD in air, indicating formation of Ag-NPs. In conclusion, the net neutralization in aqueous phase was sufficient to circumvent dissolution of the fresh formed NP via oxidation by the embedded nitric acid (induced by Birkeland-Eyde process), and a net formation of NPs is observed, even for GD in the air.

Figure 4 shows electronic images of the formed Ag-NPs under different discharge times. The neglectful variation of the mean average size observed between 5 and 15 min for DBD-Jet treatment, cf. Figures 4a and 4b, allows for interpretation on the mass transport process after metallic cation reduction on the plasma/liquid interface. In the context of particle nucleation and growth, it indicates that growth process had finished within initial 5 min whereas nucleation continues progressively, given that the NP concentration increases progressively as indicated by increased UV-Vis absorbance from 5 to 15 min. A continuous nucleation process, in conjunction with a neglectful particle growth, may only occur if these two processes take place spatially at different zones on the solution, because these processes depend, in principle, solely on the concentration of reduced silver (Ag^0).

Plasma effluent flow and the acidification rates

Table 2 shows contents of incorporated protons (H^+_{aq}) into the liquid phase and the acidification rate for each plasma treatment (see Supplementary Information (SI) section for detailed calculation). GD-air promotes the fastest acidification rate; it injects protons into solution with a global average rate equal to 293×10^{-12} mol s^{-1}. Alternatively, GD-He promotes a reduction on the aqueous proton content because it promotes a net increase on the aqueous OH^- content; thus, the negative rate in Table 2 denotes basification instead of acidification.

Table 2. Linking the electrolyte pH variation with the bulk variation (Δn) on the protons amount (Δn of $[H^+]$), computed as the difference between the initial and final $[H^+]$, see details on the SI section

Plasma edge	Exp.	Δn of H^+ ($\times 10^{-9}$) / mol	Average rate of acidification ($\times 10^{-12}$) / (mol s^{-1})
Air/air	GD-air	264.00	293.34
Air/He	DBD-Jet	0.49	0.50
He/He	GD-He	–0.50	–0.55

GD: glow discharge; DBD-Jet: dielectric barrier discharge with jet effect. $AgNO_3$ electrolyte treated for 15 min, and a 4.2 mL volume of electrolyte was used.

As a general observation, a very local plasma/liquid interaction in the air-containing atmosphere promotes substantial acidification of the entire solution, whereas, in the helium atmosphere, it promotes a basification. This ability of the gas composition on the plasma/gas to

modulate injection or extraction of protons from the self-ionization of water indicates that, at least, two independent processes are driving the global pH. They are: (*i*) the basification process described by second-order reaction (equation 2) and (*ii*) the acidification process that depends on the presence of air in the plasma/gas interface.

A second general observation for the air-containing gas phase, different plasmas sources promote solution acidification, but with considerably different rates; the mild acidification for the DBD-Jet plasma is contradictory when compared to the fast acidification for a GD-Jet plasma observed by Rumbach *et al.*[38] For this reason, we analyze in detail both experimental setups. While Rumbach's jet-plasma is generated with 30 sccm of argon jet-gas flow (180 μm inner jet diameter), this work uses 1000 sccm of helium (1300 μm inner jet diameter). Considering these values, a larger plasma flux (flow / area) is expected for our experiments. We hypothesize that a larger plasma flux promotes dissolution of the acid anions ($NO/NO_2/NO_3^-$ produced by Birkeland-Eyde process) that is generated with a constant frequency (580 Hz in this work) in the plasma edge. The smaller the initial educts content is, the slower is the acidification rate of water body. If this rationalization is correct, then the acidification rate for DBD-Jet is dependent on the jet-gas flow.

The above-mentioned hypothesis is confirmed by measuring the pH before and after treatment for 15 min with different jet-gas flows. Figure 5 shows that pH only undergoes a significant change if a jet-gas flow lower than 500 sccm is used. Above 500 sccm, precursors of the acid anions, generated at the plasma edge, are considerably diluted and reduce the acidification rate via absorption through liquid/gas interface, resulting in almost any proton (ΔH^+, Figure 5, vertical axis on the right) incorporation into the liquid. In addition, the number of protons incorporated into solution within 15 min is much higher for GD-plasma (264×10^{-9} mol) than for DBD-Jet plasma (20×10^{-9} mol, established with 50 sccm of jet flow). The intrinsic highest proton incorporation observed for GD-air electrode originates, presumably, from continuous accumulation of acid precursors in the *quasi*-static gas phase (15 sscm) instead of their dilution, as were for DBD-Jet (50 sccm).

The steep decrease of the bulk solution pH, as shown in Figure 3b and quantified in Table 2, was found to be persistent over time; which means that the low pH, over 4, measured immediately after GD treatment, remained even a day after. In this work, the final thermodynamic stable state referred is defined within this 24 h. The persistent low pH indicates that an acid had been permanently incorporated into the bulk liquid. We suspect that both nitrous acid (mild acid, HNO_2, ca. $10^{-3.4}$) and nitric acid (strong acid, HNO_3, k ca. $10^{1.4}$) are incorporated into the liquid water. It was identified the presence of nitrite ions (NO_{2aq}^-), by adding Griess reagent into the fresh plasma-treated solution, which indicates the presence of nitrous acid (HNO_2). Furthermore, a day after, the content of nitrite ions (NO_{2aq}^-) was decreased while pH remained almost stable, see SI section. We suspect that it could be related to an unknown slow aqueous kinetics to reach a truly final stable state after the plasma "perturbation" via generations of several activated-water species. This point must be addressed in future. With respect to the original work of Birkeland,[51] nitrogen oxide (NO) is produced via Birkeland-Eyde process in a torch-plasma fed with air; thereafter, it is oxidized to nitrogen dioxide (NO_2) which readily become acid when dissolved in water ($3NO_{2gas} + H_2O \rightarrow 2HNO_{3aq} + NO_{gas}$). A cautious inspection on the original work of Birkeland[51] reveals that after leaving the torch-like device at around 600-700 °C, the air-based plasma effluent is rapidly cooled down by 50 °C and so enters the absorption-system where it reacts with the water. There are strong indications that the cooling section of the Birkeland-Eyde process (or absorption-system in the own words of Birkeland)[51] is an analogue to the acidification noted by Rumbach *et al.*[38] in the second vessel; and, also, analogous to the stagnation plasma effluents (gas / liquid interface) observed in our work. It is important to mention that the composition of effluents of Birkeland's torch-plasma is not precisely known but, we believe, it must retain some equivalence to the plasma effluents from our experiments with glow discharge in the air.

Fortunately, in a recent study with plasma jet containing shielded plasma-edge, Schmidt-Bleker *et al.*[37] identified, employing Fourier transform infrared (FTIR), long-lived species such as NO_2, N_2O_5, N_2O and HNO_3 in the effluents of the plasma edge. It is possible to correlate the composition of plasma effluent studied by Schmidt-Bleker *et al.*[37] with the expected composition for the plasma effluents obtained with our DBD-Jet device. The dependence of acidification on the jet flow, as shown in Figure 5, suggests that absorption of NO_2/HNO_3 by the liquid occurs in the large gas/liquid area, instead of the small plasma/liquid contact. In view of that, the primary impact of an enlarged effluent flux in jet-plasma is a dilution of the Birkeland-Eyde process-derived products (NO_2/HNO_3) along the plasma edge and over the liquid surface. For both cases, the higher the plasma-effluent flow is, the more diluted the acid-precursor species on both the plasma edge and gas/liquid interface are; if considered that the effluent of electrochemical plasma acidifies the water in a second vessel,[38] our perception of gas/liquid interface being decisive for the liquid uptake of the acid is consistently increased.

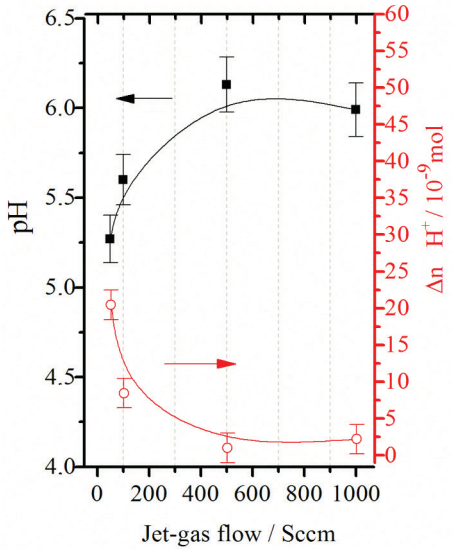

Figure 5. Variation in the pH of pure water with the helium flow during DBD-Jet treatment. ΔH^+ stands for the difference between the initial and final (after 15 min of treatment) amounts of protons in pure water.

Results of computational experiments: kinetic model for the nano-sized electrochemical reactor

In this section, we present a kinetic model applied to a very thin layer of liquid beneath the PLI. Such layer defines a small volume, ca. 10^{-9} L, termed as nano-sized electrochemical reactor, see sketch in Figure 6c. All the reactions that consume hydrated electrons occurs within this nano-volume. The aim of this section is to study the reaction pathways of the hydrated electrons and correlate the findings with the basification observed for GD in the helium.

In the kinetic model, we assume that solely reactions on equations 1 and 2 consume the hydrated electrons and that the volume for the nano-reactor does not change over time. The latter boundary condition assumes that diffusional flows of hydrated electrons is neglected within the time scale for completing the chemical reaction. This argument bases on the supporting data Table S1 (SI section). Length scales for diffusion of e_h^- that corresponds to variations of only 1% on the nano-reactor volume develops at time scale (between 6.4×10^{-9} to 0.64×10^{-9} s) very similar to the completion of the chemical reaction, i.e., 0.2×10^{-9} s as observed in Figure 7. Finally, temporal evolution for concentration of e_h^- (E) and silver cations (A) during the pulsed discharger is described, respectively, by equations 3 and 4.

$$\frac{dE}{dt} = -\left\{v_{Ag} + v_{SOR}\right\} \quad (3)$$

$$\frac{dA}{dt} = -v_{Ag} \quad (4)$$

where the rate for the silver reduction (v_{Ag}) and second-order recombination (v_{SOR}) reactions are given, respectively, by equations 5 and 6.

$$v_{Ag} = k_1 AE \quad (5)$$

$$v_{SOR} = 2k_2 E^2 \quad (6)$$

The equations 3 and 4 form together a set of ordinary differential equations that was solved using a numerical method. The applied boundary condition includes initial concentration for silver cations equal to the bulk concentration (i.e., 0.002 mol L^{-1}) whereas the initial concentration for the e_h^- is idealized to be instantaneously released to the liquid. Figure 6 summarizes part of the procedure used to estimate initial concentration of the hydrated electrons. As mentioned in the Experimental section, we had measured solely the potential at the PLI, but the pulse of current is needed to estimate the moles of electrons that effectively become e_h^-. Inspired in the work of Shirai *et al.*[53] that measured the current between the terminals of a resistor with 100 Ω, we decided to use the same value of resistance (R) to strive obtaining the current waveform via vector transformation where the reciprocal of 100 Ω is multiplied by 0.1% of the potential in Figure 2. This way, we are considering that the terminal of the emulative resistor suffers a percentage of the plasma potential variation, which effectively resembles the experiments made in real life by Shirai *et al.*[53] The resulted pulse of current is shown in Figure 6a. To obtain the quantity of electrons that effectively cross the PLI, we considered that solely electrons carry out all the current, i.e., electrons are the unique charge carrier crossing the PLI; secondly, we integrate the negative section of the current waveform, see Figure 6b that schemes the integrated part and shows the total charge obtained 0.848 μC; thirdly, we apply the first law of Kirchhoff to the PLI, thus, the same charge observed in the plasma phase must be observed in the liquid phase. Under the light of this consideration, the quantity of e_h^- is easily obtained by dividing 0.848 μC by the charge of single electron ($1.602\ 10^{-19}$ C), leading to the value of 8.79 pmols of e_h^- *per* cathodic discharge; finally, initial concentration of e_h^- is obtained dividing this value by the volume of the nano-reactor, resulting in a value of 0.661 mol L^{-1}. All this information is compiled into Table 3. In this approach, all the charge related to one single cathodic discharge (8.79 pmols) is assumed to be instantaneously injected into the nano-sized reactor, which is not realist, but sufficient for a preliminary evaluation, given that the discharge last 0.15 ms (150,000 ns) whereas the time scale for the reactions is much faster (ca. 0.2 ns).

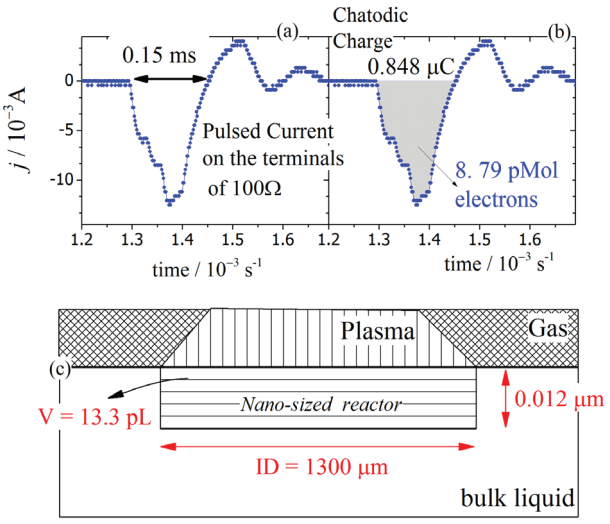

Figure 6. (a) Hypothetical current observed in the plasma / liquid interface during a single pulsed cathodic discharge; (b) integration to obtain the quantity of electrons injected into the liquid and (c) a two-dimensional sketch of the idealized nano-sized electrochemical reactor formed beneath the plasma-liquid interface.

Table 3. Boundary conditions to solve kinetic model

Quantities *per* cathodic discharge	
Mol of electrons / pmol	8.79
Concentration of e_h^- into the volume of the nanoreactor / (mol L^{-1})	0.66
Nanoreactor dimension	
Electron penetration (P)[23] / nm	12.00
Inner diameter (ID) / μm	1,300.00
Contact area plasma/liquid ($[\pi(ID)^2 / 4]$) / (10^{-6} m^2)	1.33
Volume of nanoreactor ($P \times [\pi(ID)^2 / 4]$) / pL	13.30

Figure 7 shows the temporal evolutions for the local concentrations of silver cations and hydrated electrons, after taking into consideration the idealized condition described above. Several initial concentrations of silver cations were tested and overall three kinetics scenarios were found in Figure 7. The first two diametrically opposite scenarios are depicted in Figure 7a for low and Figure 7d for sufficiently high silver cation concentration. When a low concentration of Ag^+ is employed, as 0.002 mol L^{-1} used in this work, all content of Ag^+ ions in the nano-sized reactor is immediately consumed after electron injection, leading to a negligible rate of silver reduction reaction, see Figure 7e. In this first scenario, the hydrated electrons are consumed primarily by the second-order recombination reaction. The second scenario occurs when sufficiently high initial concentration of silver cation is used, which guarantee that transients for the rate of silver reduction reaction largely exceeds the rate of the second-order recombination reaction, see Figure 7h. As a result, the initial concentration of Ag^+ is decreased but not fully depleted within the volume of the nano-sized reactor, whereas the concentration of hydrated electrons attains zero, see Figure 7d, which in turn indicates the injected electrons is majorly consumed by the silver reduction reaction. Finally, the intermediate scenarios embrace all the other cases where both the concentrations, see Figures 7b and 7c, and the rate of reaction, Figures 7f and 7g, for silver reduction and second-order recombination reactions evolve with balanced values. In such scenarios, all content of the injected electrons are balanced between these two reactions.

Despite three-scenarios observed in Figure 7 being generalist, we need to test how realistic the description is since, indeed, the initial concentration of e_h^- is unrealistically high because, as mentioned before, it was considered an instantaneous release of all the charge accumulated along 0.15 ms (150,000 ns) in the cathodic discharge. Ideally, the truly instantaneous release of electrons has to consider charge integration over time window as narrow as the time scale that kinetics attains steady state at ca. 10^{-8} s (10 ns). However, we would have to establish a methodology of analysis that goes beyond the scope of this current work. Alternatively, Figure 8 shows, for a single discharge, both the charge accumulated along the discharge, Figure 8b, and the mols of electrons crossing the PLI, see Figure 8c. In addition, Figure 8c counts the mols of silver cations storage into the nano-reactor volume considering three different bulk concentrations of silver cations (10, 0.8 and 0.002 mol L^{-1}). For the bulk concentration used in this work, 0.002 mol L^{-1}, the quantity of e_h^- overpasses the quantity of cations storage into the nano-reactor, corroborating the scenario 1 described in the Figure 7a. Furthermore, for the current waveform of this work, it would be necessary to use 0.8 mol L^{-1} of bulk silver cations to guarantee a quantity of e_h^- always below the quantity of cations into the nano-reactor during a single discharge.

The basification observed for our results with glow discharge using helium in the gas phase, Figures 3c and 3d, is explained under the light of the findings in Figures 7 and 8. As we used a sufficiently low Ag^+ concentration, the local Ag^+ concentration immediately depletes to almost zero, like the evolution in Figure 7a. In this scenario, localized e_h^- is majorly consumed by the second-order recombination reaction, rather than by the silver reduction reaction, leading to substantial localized production of OH_{aq}^- that, over time, accounts for the net increase of the bulk pH. An alternative to this explanation is seen in Figure 8c that exhibits the quantity of electrons crossing the PLI plus the horizontal lines that represents the quantity in mols of silver cations storage into the reactor beneath PLI. If considered

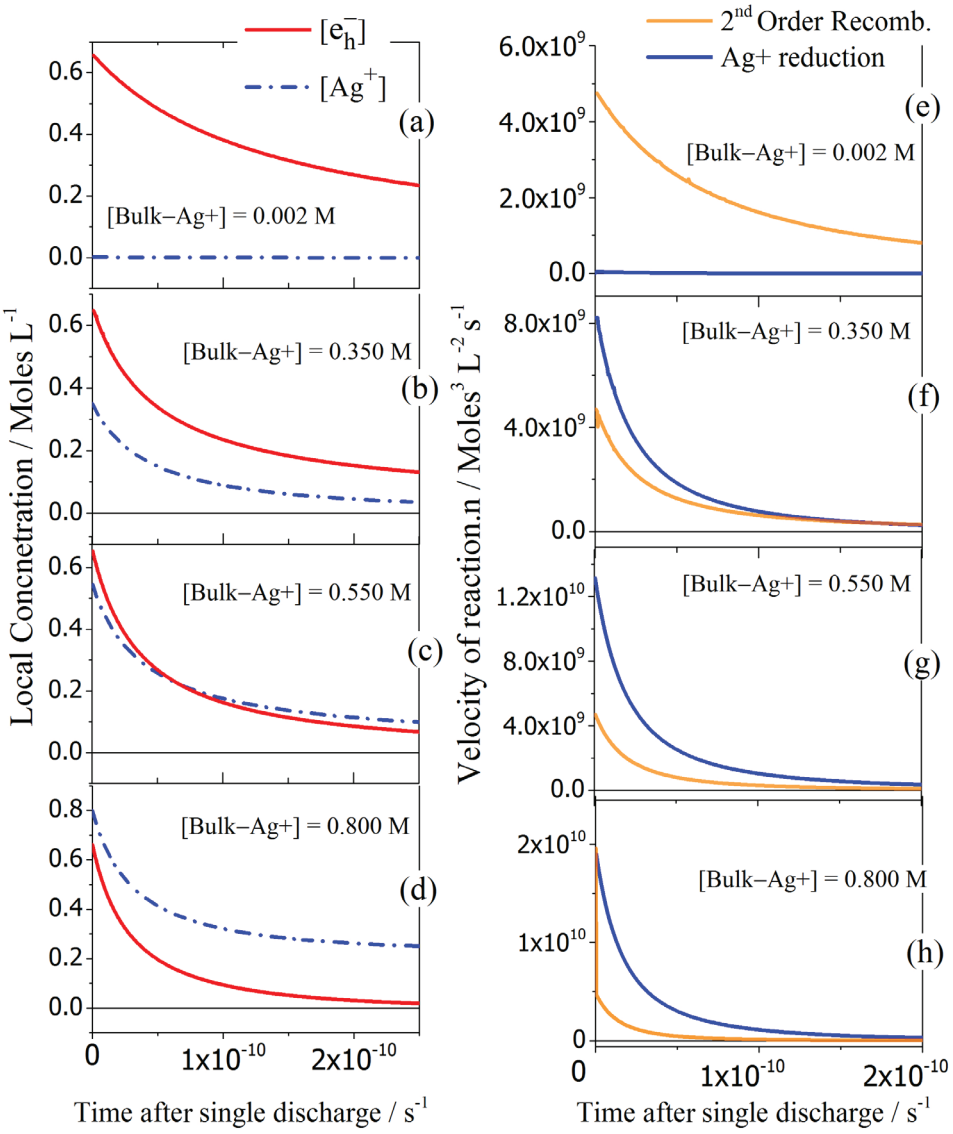

Figure 7. First column shows the temporal evolution of local concentration for the silver cations (Ag^+) and hydrated electrons (e_h^-) obtained by computational experiments using equations 3 and 4; and considering 0.661 mol L^{-1} as initial concentration for e_h^- combined with different initial concentration for Ag^+: (a) 0.002; (b) 0.350; (c) 0.550 and (d) 0.800 mol L^{-1}. Second column shows rate of reaction for silver reduction and second-order recombination reactions using 0.661 mol L^{-1} as initial concentration for e_h^- combined with different initial concentration for Ag^+: (e) 0.002; (f) 0.350; (g) 0.550 and (h) 0.800 mol L^{-1}.

0.002 mol L^{-1}, the same initial cation concentration used in this work, the mols of electrons overpass the mols of silver cations storage into the reactor beneath PLI at the very early stage of the discharge. This indicates that the rate of the silver reduction reaction becomes limited by diffusional fluxes at the later stages of the discharge. For this reason, e_h^- starts to react via second-order recombination (see equation 2), and the substantial production of localized OH_{aq}^- results, over time, in a global rise of the bulk pH.

Plasma-induced reduction reaction mechanism

The mechanism of reduction reaction underneath the PLI depends on the nature of the noble cation. For instance, gold cations are propitious to be reduced both by hydrated e_{aq}^- and H_2O_2, whereas silver cations could only be reduced by e_{aq}^-. Considering the polarity selectivity of both e_{aq}^- (only produced in cathodic electrochemical plasma) and H_2O_2 (only produced in anodic electrochemical plasma), as mentioned in the Introduction section, it is possible to re-interpret the findings of Shirai *et al.*[54] These authors tested the polarity effect on the reduction reaction, and observed that silver reduction only occurs for cathodic plasma, whereas golden cations were reduced for either plasma polarity. The golden cation reduction in a polarity where electrons are repelled from the PLI (in anodic plasma) is justified by the presence of H_2O_2 that readily reduces gold.

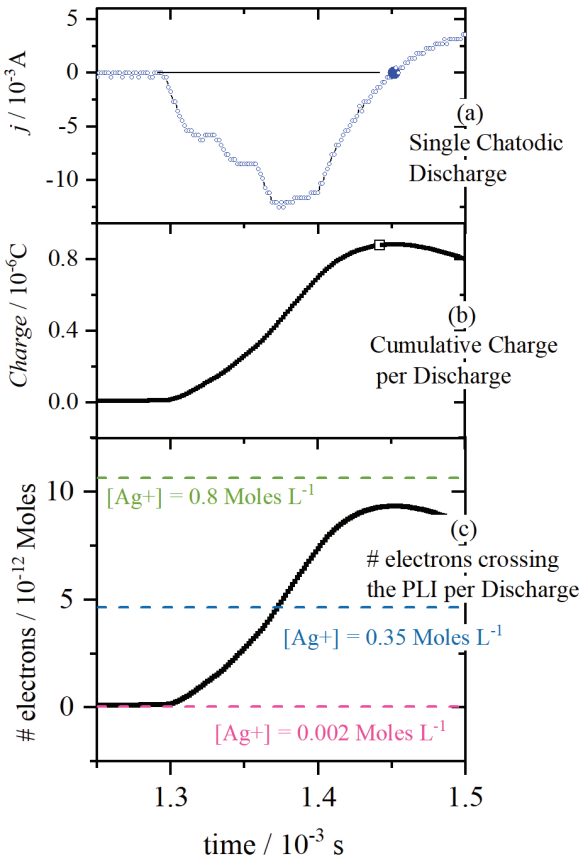

Figure 8. (a) Hypothetical profile of the current during a pulsed discharge used to calculate both (b) the cumulative charge of electrons and (c) the quantity of electrons in terms of mols crossing the plasma/liquid interface within a single discharge. In Figure 8c, the horizontal lines indicate the quantity in mols of silver cations (Ag^+) that are stored into the volume of the nano-reactor (13.3 pL) beneath the liquid surface considering three different bulk concentrations of silver cations (10, 0.8 and 0.002 mol L^{-1}).

Additionally to the reduction mediated either by e^-_{aq} [1,2,23,55,56] or by H_2O_2,[57,58] reduction mediated by hydrogen radical (produced via irradiation of neutral radicals of the plasma) is suggested by Kaneko *et al.*[7] and defended by Bruggeman and co-authors.[59] In principle, hydrogen radical ($H^\bullet$) is produced upon plasma phase via hydrogen dissociation by vacuum ultraviolet (VUV, equation 7):

$$h\nu + H_2 \rightarrow 2H^\bullet \quad (7)$$

or via water VUV-photolysis in plasma phase which also produces hydroxide radicals ($OH^\bullet$). Equation 8 was cited here.

$$h\nu + H_2O \rightarrow OH^\bullet + H^\bullet \quad (8)$$

and according to the analysis of Ghosh *et al.*[55] hydroxide radicals $OH^\bullet$ have more favorable energy of solvation by the water phase than does hydrogen radical ($H^\bullet$) leading to a negligible concentration of $H^\bullet$ on the topmost layers of the water surface. Thus, only $OH^\bullet$ is hereby considered as scavenger for e^-_{aq} (equation 9):

$$e^-_h + OH^\bullet \xrightarrow{k5=3.0\times10^{10}\ M^{-1}s^{-1}} OH^- \quad (9)$$

Bruggeman and co-authors[59] defends that $OH^\bullet$ and e^-_{aq} are in equal concentration in the water topmost layers in contact with the torch-plasma. If so, the local concentrations of the reactant and the rate of reaction evolve over time accordingly to the intermediate scenario described in this work, similar to that in Figures 7c and 7g. The injected electrons are balanced majorly between two reactions, namely scavenger reaction, displayed by equation 9, and the second-order recombination reactions (see equation 1), whereas the local concentration of silver cation depletes because the initial bulk concentration used by the authors is low. However, we are not totally convinced whether is even possible to presume the local concentration of $OH^\bullet$ and e^-_{aq} without any previous information of yields for these species in the torch-plasma used by the authors. Furthermore, it is speculative a direct comparison between a torch-plasma and an electrochemical plasma once the PLI for each case are essentially different: a non-electrified PLI promotes zero net current through PLI for torch-plasma whereas an electrified PLI forces a net current to cross the PLI which is termed electrochemical plasma. As seen in theoretical part, the localized net current at the PLI generates abnormally high local concentration of e^-_{aq} within a time scale as narrow as 1 ns (10^{-9} s), enabling an overall kinetic domination of the second-order recombination reaction.

Mechanism of NP formation and the reaction pathways for the hydrated electron

As observed in the Figure 4, the negligible variation of mean NP size over time indicates a continuous nucleation process in conjunction with a neglectful particle growth. This fact may only occur if nucleation and growth take place spatially at different zones in the solution. Thus, we proposed that nucleation occurs at the topmost layers underneath the plasma / liquid interface where a high content of Ag^0 exists. As concentration of Ag^0 is depleted downward liquid surface, NPs stop growing during their diffusion into bulk liquid phase. In addition, the scenario of spatially-dependent nucleation and growth is consistent with our interpretation of lacking Ag^0 accreting in presence of high acidification process. Within topmost layers underneath plasma/liquid interface, nucleation does not occur in presence of high content of nitric acid, and also it does not occur at bulk liquid because Ag^0 concentration is very low at such spatial position.

The acidification is a concomitant and independent process with respect to the NP synthesis and depends on the presence of both O_2 and N_2 (air) in the plasma edge, attributed to be the Birkeland-Eyde process of acidification by nitric acid. Different plasma sources might fulfill this requirement and promote acidifications as were observed in this work for either DBD-(He)Jet or GD-air. We suggest that nitric acid interferes with the accretion of reduced silver, thereby preventing NP nucleation. Furthermore, we suggest that nitric acid fixation in liquid phase occurs majorly through the gas / liquid interface. All the processes accompanying the plasma-induced NP synthesis are schematically depicted in Figure 9.

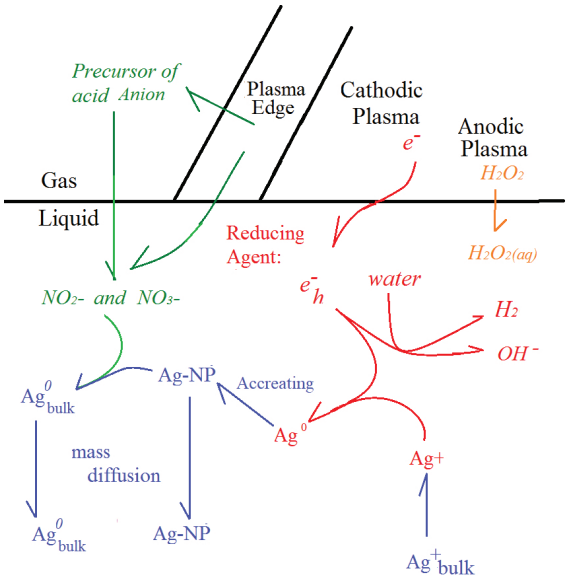

Figure 9. Scheme for the reaction pathways for the hydrated electrons and for the mechanism of NP formation that are drastically affected by an independent process of acidification.

Figure 9 also sketches the reaction pathways for the hydrated electrons. From a fundamental perspective, the pathways for e^-_{aq} could only be perceived in a complete suppression of the Birkeland-Eyde induced acidification once it hides the basification induced by the second-order recombination reaction of the e^-_{aq}. As demonstrated in this work, an effective suppression of the Birkeland-Eyde acidification is obtained by the usage of a nitrogen-free gas-plasma interface (plasma edge) such as a helium *quasi*-static atmosphere for contactless GD.

Regarding the plasma-induced reduction reactions, silver ions are reduced at the volume within the topmost water layers (termed here as nano-sized reactor) rich in e^-_{aq}. If the acidification process by nitric acid uptake are much faster than the silver reduction reaction, the rate of silver sub-nanocluster accretion decreases, resulting in a negligible rate of nucleation and overall negligible net nanoparticle growth. Conversely, if the acidification process is effectively suppressed, the net effect of reduction reactions underwent within the topmost water layers becomes globally perceived via the basification that accompanies the Ag-NPs synthesis. The silver reduction together with OH^-_{aq} production indicates dual reaction pathway for the e^-_{aq} which either react via second-order recombination reaction (see equation 2) or via scavenger-like such as the silver cations reduction (see equation 1).

For discharge directly in or in contact with air-containing gas phase, some successful strategies to circumvent acidification while synthetizing Ag-NPs were identified: (*i*) high helium gas flow in plasma-jet; and (*ii*) the usage of basified electrolyte (intentional addition of any hydroxide). Furthermore, we also foresee that alternatives such as (*iii*) usage of buffer solutions as well as (*iv*) ventilation of the gas/liquid interface could equally be able to prevent acidification by nitric acid. For a technological goal, those strategies must be sufficient to improve the rate of NP synthesis.

Conclusions

Given the electrochemical effect in liquid phase, the discharge over a liquid surface is termed electrode, and the contact discharge/liquid termed plasma / liquid interface (PLI). Two plasma sources, dielectric barrier discharge with jet effect (DBD-Jet) and glow discharger (GD), manifested similar capabilities of reducing silver cations at the PLI provided that the Birkeland-Eyde acidification process was suppressed. The results with varied jet flow indicate that the cation of the strong acid precursor (presumably NO^-_2 and NO^-_3) formed on the plasma edge is absorbed by the electrolyte primarily through the liquid / gas phase. We propose that the acidification process interfere in the NP nucleation because reduced Ag^0 does not accrete effectively as any eventually nucleated NP-seeds promptly dissolve in nitric acid solution.

Among the strategies found to circumvent effectively the acidification rate, even in the presence of air in the plasma edge (gas/plasma interphase), are (*i*) the fast helium jet flow for DBD-Jet and (*ii*) the usage of alkaline electrolyte (via intentional addition of hydroxide) for GD in the air. Besides, acidification could be completely suppressed if nitrogen-free composition is used in both gas and plasma phases. In this work, we employed helium in both gas and plasma phases to suppress the acidification completely (GD in He); and, turned out that pH of the bulk liquid interestingly dislocated toward the large values on the pH scale. The basification

observed in the helium-based GD is interpreted as a fierce experimental evidence for the second-order recombination reaction of the hydrated electrons (e^-_{aq}).

The simultaneous silver reduction and OH^-_{aq} production strongly indicate a dual pathway for e^-_{aq} which either react via second-order recombination reaction or reacts via silver cations reduction. We proposed a kinetic model for the region beneath the PLI, termed nano-reactor; and, the concentrations of Ag^+ and e^-_{aq} over discharge evolution were assessed via computational aided simulations. We applied the first law of Kirchhoff on the current crossing the PLI, in turn, enabling to estimate the initial concentration of e^-_{aq} from a current waveform for a single pulsed discharge. Such approach must not be applicable to a torch-plasma in contact with the liquid surface as the discharge in this device is between two metallic electrodes, instead of between a metallic electrode and a liquid surface electrode as usually defined for an electrochemical discharge. In our model, the localized net current at the PLI for an electrochemical discharge generates an abnormally high local concentration of e^-_{aq} within a time scale as narrow as 1 ns (10^{-9} s), enabling an overall kinetic domination of the second-order recombination reaction when used an initially low concentration of a scavenger, silver cations in this case.

Several other processes, beyond electro-reduction in the liquid region underneath the PLI, develop on the other plasma-related interfaces. Occasionally, those independent processes may interplay. This work elucidates a vivid case on how a process developing either on plasma / liquid or liquid/gas phases affect the net reduction of the silver cations on the region underneath the PLI.

Supplementary Information

Supplementary data (calculus for the time scales for diffusion of hydrated electrons and calculus for the experimental rate of acidification) are available free of charge at http://jbcs.sbq.org.br as a PDF file.

Acknowledgments

This project was funded by the National Council for Scientific and Technological Development (CNPq No. 306087/2013-8) and the Coordination of Higher Education Personnel Training (CAPES No. 403230/2013-6). The authors acknowledge the support from the National Institute of Surface Engineering (CNPq-465423/2014-0), in particular, A. M. L. (CNPq-381050/2017-3). F. J. C. F. (CNPq-155881/2017-5) thanks the Graduate Program in Chemical Engineering from UFRN for sponsoring this publication. A. M. L. acknowledges comments from several colleagues from the plasma community as their judgment aided refining the interpretations of this work.

References

1. Rumbach, P.; Bartels, D. M.; Sankaran, R. M.; Go, D. B.; *Nat. Commun.* **2015**, *6*, 7248.
2. Richmonds, C.; Witzke, M.; Bartling, B.; Lee, S. W.; Wainright, J.; Liu, C.-C.; Sankaran, R. M.; *J. Am. Chem. Soc.* **2011**, *133*, 17582.
3. Richmonds, C.; Sankaran, R. M.; *Appl. Phys. Lett.* **2008**, *93*, 131501.
4. Chiang, W.-H.; Sankaran, R. M.; *Appl. Phys. Lett.* **2007**, *91*, 121503.
5. Chen, Q.; Kaneko, T.; Hatakeyama, R.; *Appl. Phys. Express* **2012**, *5*, 086201.
6. Chen, Q.; Kaneko, T.; Hatakeyama, R.; *Chem. Phys. Lett.* **2012**, *521*, 113.
7. Kaneko, T.; Takahashi, S.; Hatakeyama, R.; *Plasma Phys. Controlled Fusion* **2012**, *54*, 124027.
8. Mariotti, D.; Sankaran, R. M.; *J. Phys. D: Appl. Phys.* **2011**, *44*, 174023.
9. Mariotti, D.; Sankaran, R. M.; *J. Phys. D: Appl. Phys.* **2010**, *43*, 323001.
10. Kortshagen, U. R.; Sankaran, R. M.; Pereira, R. N.; Girshick, S. L.; Wu, J. J.; Aydil, E. S.; *Chem. Rev.* **2016**, *116*, 11061.
11. Huang, X. Z.; Zhong, X. X.; Lu, Y.; Li, Y. S.; Rider, A. E.; Furman, S. A.; Ostrikov, K.; *Nanotechnology* **2013**, *24*, 095604.
12. de Vos, C.; Baneton, J.; Witzke, M.; Dille, J.; Godet, S.; Gordon, M. J.; Sankaran, R. M.; Reniers, F.; *J. Phys. D: Appl. Phys.* **2017**, *50*, 105206.
13. Hieda, J.; Saito, N.; Takai, O.; *J. Vac. Sci. Technol* **2008**, *26*, 854.
14. Heo, Y. K.; Bratescu, M. A.; Ueno, T.; Saito, N.; *J. Appl. Phys.* **2014**, *116*, 024302.
15. Bratescu, M. A.; Cho, S.-P.; Takai, O.; Saito, N.; *J. Phys. Chem. C* **2011**, *115*, 24569.
16. Su, N.; Hu, X.; Zhang, J.; Huang, H.; Cheng, J.; Yu, J.; Ge, C.; *Appl. Surf. Sci.* **2017**, *399*, 403.
17. Sudare, T.; Ueno, T.; Watthanaphanit, A.; Saito, N.; *Phys. Chem. Chem. Phys.* **2015**, *17*, 30255.
18. Lu, Y.; Ren, Z.; Yuan, H.; Wang, Z.; Yu, B.; Chen, J.; *RSC Adv.* **2015**, *5*, 62619.
19. Bilik, N.; Greenberg, B. L.; Yang, J.; Aydil, E. S.; Kortshagen, U. R.; *J. Appl. Phys.* **2016**, *119*, 243302.
20. Liu, J.; Chen, Q.; Li, J.; Xiong, Q.; Yue, G.; Zhang, X.; Yang, S.; Liu, Q. H.; *J. Phys. D: Appl. Phys.* **2016**, *49*, 275201.
21. Velusamy, T.; Liguori, A.; Macias-Montero, M.; Padmanaban, D. B.; Carolan, D.; Gherardi, M.; Colombo, V.; Maguire, P.; Svrcek, V.; Mariotti, D.; *Plasma Processes Polym.* **2017**, e1600224.

22. Liu, J.; He, B.; Chen, Q.; Liu, H.; Li, J.; Xiong, Q.; Zhang, X.; Yang, S.; Yue, G.; Liu, Q. H.; *Electrochim. Acta* **2016**, *222*, 1677.
23. Rumbach, P.; Xu, R.; Go, D. B.; *J. Electrochem. Soc.* **2016**, *163*, F1157.
24. Gopalakrishnan, R.; Kawamura, E.; Lichtenberg, A. J.; Lieberman, M. A.; Graves, D. B.; *J. Phys. D: Appl. Phys.* **2016**, *49*, 295205.
25. Goodman, J.; Hickling, A.; Schofield, B.; *J. Electroanal. Chem.* **1973**, *48*, 319.
26. Kang, W. S.; Hur, M.; Song, Y.-H.; *Appl. Phys. Lett.* **2015**, *107*, 094101.
27. Bruggeman, P. J.; Kushner, M. J.; Locke, B. R.; Gardeniers, J. G. E.; Graham, W. G.; Graves, D. B.; Hofman-Caris, R. C. H. M.; Maric, D.; Reid, J. P.; Ceriani, E.; Rivas, D. F.; Foster, J. E.; Garrick, S. C.; Gorbanev, Y.; Hamaguchi, S.; Iza, F.; Jablonowski, H.; Klimova, E.; Kolb, J.; Krcma, F.; Lukes, P.; Machala, Z.; Marinov, I.; Mariotti, D.; Thagard, S. M.; Minakata, D.; Neyts, E. C.; Pawlat, J.; Petrovic, Z. L.; Pflieger, R.; Reuter, S.; Schram, D. C.; Schröter, S.; Shiraiwa, M.; Tarabová, B.; Tsai, P. A.; Verlet, J. R. R.; Woedtke, T. V.; Wilson, K. R.; Yasui, K.; Zvereva, G.; *Plasma Sources Sci. Technol.* **2016**, *25*, 053002.
28. Chen, Q.; Li, J.; Li, Y.; *J. Phys. D: Appl. Phys.* **2015**, *48*, 424005.
29. Hickling, A.; Ingram, M. D.; *Trans. Faraday Soc.* **1964**, *60*, 783.
30. Sengupta, S. K.; Singh, O. P.; *J. Electroanal. Chem.* **1994**, *369*, 113.
31. Sengupta, S. K.; Singh, R.; Srivastava, A. K.; *J. Electrochem. Soc.* **1998**, *145*, 2209.
32. Akolkar, R.; Sankaran, R. M.; *J. Vac. Sci. Technol* **2013**, *31*, 050811.
33. Glasstone, S.; Hickling, A.; *J. Chem. Soc.* **1934**, 1772.
34. Liu, J.; He, B.; Chen, Q.; Li, J.; Xiong, Q.; Yue, G.; Zhang, X.; Yang, S.; Liu, H.; Liu, Q. H.; *Sci. Rep.* **2016**, *6*, 38454.
35. Locke, B. R.; Shih, K.-Y.; *Plasma Sources Sci. Technol.* **2011**, *20*, 034006.
36. Garrett, B. C.; Dixon, D. A.; Camaioni, D. M.; Chipman, D. M.; Johnson, M. A.; Jonah, C. D.; Kimmel, G. A.; Miller, J. H.; Rescigno, T. N.; Rossky, P. J.; Xantheas, S. S.; Colson, S. D.; Laufer, A. H.; Ray, D.; Barbara, P. F.; Bartels, D. M.; Becker, K. H.; Bowen, K. H.; Bradforth, S. E.; Carmichael, I.; Coe, J. V.; Corrales, L. R.; Cowin, J. P.; Dupuis, M.; Eisenthal, K. B.; Franz, J. A.; Gutowski, M. S.; Jordan, K. D.; Kay, B. D.; LaVerne, J. A.; Lymar, S. V.; Madey, T. E.; McCurdy, C. W.; Meisel, D.; Mukamel, S.; Nilsson, A. R.; Orlando, T. M.; Petrik, N. G.; Pimblott, S. M.; Rustad, J. R.; Schenter, G. K.; Singer, S. J.; Tokmakoff, A.; Wang, L.-S.; Zwier, T. S.; *Chem. Rev.* **2005**, *105*, 355.
37. Schmidt-Bleker, A.; Winter, J.; Bosel, A.; Reuter, S.; Weltmann, K.-D.; *Plasma Sources Sci. Technol.* **2016**, *25*, 015005.
38. Rumbach, P.; Witzke, M.; Sankaran, R. M.; Go, D. B.; *J. Am. Chem. Soc.* **2013**, *135*, 16264.
39. Bruggeman, P.; Ribežl, E.; Maslani, A.; Degroote, J.; Malesevic, A.; Rego, R.; Vierendeels, J.; Ley, C.; *Plasma Sources Sci. Technol.* **2008**, *17*, 025012.
40. Gorbanev, Y.; O'Connell, D.; Chechik, V.; *Chem. - Eur. J.* **2016**, *22*, 3496.
41. Bednar, N.; Matović, J.; Stojanović, G.; *J. Electrost.* **2013**, *71*, 1068.
42. Witzke, M.; Rumbach, P.; Go, D. B.; Sankaran, R. M.; *J. Phys. D: Appl. Phys.* **2012**, *45*, 442001.
43. Sengupta, S. K.; *Plasma Sources Sci. Technol.* **2015**, *24*, 063001.
44. Polyakov, O. V.; Badalyan, A. M.; Bakhturova, L. F.; *High Energy Chem.* **2003**, *37*, 322.
45. *Scilab*, 6.0.1; ESI Group, Paris, France, 2018.
46. Schutze, A.; Jeong, J. Y.; Babayan, S. E.; Park, J.; Selwyn, G. S.; Hicks, R. F.; *IEEE Trans. Plasma Sci.* **1998**, *26*, 1685.
47. Mulvaney, P.; *Langmuir* **1996**, *12*, 788.
48. Hicks, J. F.; Miles, D. T.; Murray, R. W.; *J. Am. Chem. Soc.* **2002**, *124*, 13322.
49. Pillai, Z. S.; Kamat, P. V.; *J. Phys. Chem. B* **2004**, *108*, 945.
50. Gomes, J. F.; Garcia, A. C.; Ferreira, E. B.; Pires, C.; Oliveira, V. L.; Tremiliosi-Filho, G.; Gasparotto, L. H. S.; *Phys. Chem. Chem. Phys.* **2015**, *17*, 21683.
51. Birkeland, K.; *Trans. Faraday Soc.* **1906**, *2*, 98.
52. Kakkar, R.; Sherly, E. D.; Madgula, K.; Devi, D. K.; Sreedhar, B.; *J. Appl. Polym. Sci.* **2012**, *126*, E154.
53. Shirai, N.; Ichinose, K.; Uchida, S.; Tochikubo, F.; *Plasma Sources Sci. Technol.* **2011**, *20*, 034013.
54. Shirai, N.; Uchida, S.; Tochikubo, F.; *Jpn. J. Appl. Phys.* **2014**, *53*, 046202.
55. Ghosh, S.; Hawtof, R.; Rumbach, P.; Go, D. B.; Akolkar, R.; Sankaran, R. M.; *J. Electrochem. Soc.* **2017**, *164*, D818.
56. Rumbach, P.; Griggs, N.; Sankaran, R. M.; Go, D. B.; *IEEE Trans. Plasma Sci.* **2014**, *42*, 2610.
57. Patel, J.; Němcová, L.; Maguire, P.; Graham, W. G.; Mariotti, D.; *Nanotechnology* **2013**, *24*, 245604.
58. Mariotti, D.; Patel, J.; Švrček, V.; Maguire, P.; *Plasma Processes Polym.* **2012**, *9*, 1074.
59. Kondeti, V. S. S. K.; Gangal, U.; Yatom, S.; Bruggeman, P. J.; *J. Vac. Sci. Technol.* **2017**, *35*, 061302.

Submitted: August 15, 2018
Published online: February 6, 2019